

Geophysical Research Letters

RESEARCH LETTER

10.1029/2020GL089548

Key Points:

- Subtropical jet winter mixing barriers extend upward in response to climate change
- Eddy transport in the subtropical lower stratosphere is enhanced in the summer hemisphere
- Ozone hole recovery weakens austral polar mixing barrier in spring and summer

Supporting Information:

- Supporting Information S1
- Supporting Information S2

Correspondence to:

M. Abalos,
mabalosa@ucm.es

Citation:

Abalos, M., & de la Cámara, A. (2020). Twenty-first century trends in mixing barriers and eddy transport in the lower stratosphere. *Geophysical Research Letters*, 47, e2020GL089548. <https://doi.org/10.1029/2020GL089548>

Received 26 JUN 2020

Accepted 4 OCT 2020

Accepted article online 14 OCT 2020

Twenty-First Century Trends in Mixing Barriers and Eddy Transport in the Lower Stratosphere

M. Abalos¹  and A. de la Cámara¹ 

¹Department of Earth Physics and Astrophysics, Universidad Complutense de Madrid, Madrid, Spain

Abstract Future trends in isentropic mixing in the lower stratosphere remain largely unexplored, in contrast with other aspects of stratospheric tracer transport. This study examines trends in effective diffusivity (κ_{eff}), a measure of the potential of the flow to produce isentropic mixing, in recent chemistry-climate model simulations. The results highlight substantial reduction of κ_{eff} in the upper flanks of the subtropical jets from fall to spring, which are strengthened in response to greenhouse gas increases. This contrasts with stronger eddy transport, associated with increased wave drag in the region, peaking in summer near the critical lines. The key role of changes in tracer meridional gradients in addition to transport barriers for isentropic mixing trends is evidenced. The projected ozone recovery leads to enhanced κ_{eff} in polar austral spring and summer, associated with a weaker and shorter-lived austral polar vortex by the end of the 21st century.

Plain Language Summary As the temperature of the tropical upper troposphere increases due to continued increase in greenhouse gases, the upper flanks of the subtropical jets are reinforced, with important implications for tracer transport in the lower stratosphere. Here, we examine for the first time the future trends in isentropic mixing, a key component of tracer transport in the lower stratosphere. The results show an upward extension of the mixing barriers associated with the core of the subtropical jets in winter. On the other hand, tracer eddy transport above the subtropical jets increases in summer, due to the upward and equatorward shift of the region where Rossby waves dissipate (i.e., the critical lines). In addition, ozone hole recovery over the 21st century warms the austral polar stratosphere, weakens the polar night jet, and shifts critical lines to lower levels in summer, enhancing wave breaking and isentropic mixing in the polar lower stratosphere. Such effect overcomes the strengthening of the Southern Hemisphere polar vortex by greenhouse gas increases. These mixing diagnostics can help interpret observed trends in tracer concentrations and could be valuable in attempting to reconcile modeled and observed trends in stratospheric transport.

1. Introduction

The zonal mean tracer transport in the stratosphere, known as the Brewer-Dobson circulation (BDC), determines the distribution and variability of the chemical compounds in the stratosphere, including the radiatively active species such as ozone or water vapor. The BDC is divided into two components, the mean meridional or residual circulation, which tends to increase meridional tracer gradients between low and high latitudes, and two-way quasi-isentropic mixing, which tends to compensate for this effect and flatten out the tracer contours (Plumb, 2002). Both transport processes are closely associated with breaking waves. On one hand, Rossby and gravity wave breaking force the residual circulation by transfer of momentum to the zonal mean flow combined with the Coriolis force. On the other hand, as large-scale waves break, they lead to stirring of the air masses and quasi-isentropic mixing of chemical compounds.

A relatively large number of studies have investigated the effects of climate change on the BDC in general and on the residual circulation in particular. The results are robust across models and climate change scenarios, revealing an acceleration of the residual circulation, resulting in a reduction of the mean age of stratospheric air (Butchart, 2014). This acceleration is associated with a strengthening of the upper flanks of the subtropical jets, which modifies the conditions for wave propagation and dissipation (Garcia & Randel, 2008) by shifting the critical lines (Shepherd & McLandress, 2011). Such changes in the subtropical jets result mainly from enhanced warming of the tropical upper troposphere (World Meteorological Organization

[WMO], 2018). Specifically, thermal wind balance translates the decrease in the (positive) meridional temperature gradient in the subtropics into a weaker (negative) zonal wind shear, hence strengthening the upper flanks of the jets.

In addition to these climate change effects, recent works have highlighted an important role of ozone depletion and recovery on the BDC trends. In particular, it has been shown that the formation of the ozone hole contributed substantially to the acceleration of the BDC over the last decades of the 20th century (Abalos et al., 2019; Oman et al., 2009). The ozone hole affects the BDC by modulating the strength and duration of the austral polar vortex. Ozone accumulated in the polar lower stratosphere during winter absorbs solar radiation in spring and summer, warming the polar cap and weakening the vortex. As ozone was severely depleted over the last decades of the 20th century, the austral polar stratosphere became colder and the vortex stronger and more persistent. The westerly trends in the summer polar stratosphere shifted the critical lines upward into the stratosphere, contributing to strengthen the residual circulation. The opposite effect is expected in the ozone recovery period (McLandress et al., 2010; Oman et al., 2009), and consistently, the Southern Hemisphere (SH) polar downwelling decelerates after the year 2000 (Polvani et al., 2018, 2019).

On the other hand, there are only a few published studies to date on the future changes in isentropic mixing. The value of assessing long-term trends in isentropic mixing in addition to residual circulation advection is highlighted by recent works revealing their key role on age of air trends (Eichinger et al., 2019; Ploeger et al., 2015). This contrasts with the results of Li et al. (2012) showing little impact of mixing on mean age trends. Another example is the current debate regarding the transport mechanism behind the decrease in observed lower stratosphere northern midlatitude ozone over the last decades (Ball et al., 2018; Chipperfield et al., 2018), as the role of isentropic mixing versus vertical advection remains unclear (Orbe et al., 2020; Wargan et al., 2018). Abalos et al. (2017, 2020) examined 21st century trends in transport of a tropospheric and stratospheric tracers, respectively, and found increased quasi-horizontal eddy transport above the subtropical jets. Isentropic mixing of a tracer can be thought of as a diffusion term in the tracer continuity equation, in which the diffusion coefficient provides a spatiotemporal distribution of the efficiency of the flow to generate isentropic mixing. In this sense, the effective diffusivity (κ_{eff}) introduced by Nakamura (1996) quantifies the changes in microscale diffusion due to the large-scale stirring of tracer contours (Haynes & Shuckburgh, 2000). Abalos et al. (2019) showed that κ_{eff} trends over 1980–2000 were strongly influenced by the effect of the ozone hole in austral summer, both in a chemistry-climate model and in reanalyses. In this study we provide the first assessment of the 21st century trends in κ_{eff} in the lower stratosphere, separating the effects of climate change and ozone recovery.

2. Data and Methods

We use simulations of the Community Earth System Model (Version 1), which has the Whole Atmosphere Community Climate Model (WACCM Version 4) as the atmospheric component with interactive chemistry, fully coupled to ocean, land, and sea ice components. The horizontal resolution of WACCM is 1.9° in latitude and 2.5° in longitude, and the vertical resolution ranges from ~1.2 km near the tropopause to ~2 km near the stratopause, and the model top is around 140 km. The baseline version of is detailed in Marsh et al. (2013), with later improvements to stratospheric heterogeneous chemistry and to orographic gravity wave forcing (Garcia et al., 2017). The model version reproduces accurately the ozone hole (Solomon et al., 2015).

We analyze three types of simulations over the 21st century, which are different scenarios proposed by the International Global Atmospheric Chemistry/Stratosphere-troposphere Processes and their Role in Climate (IGAC/SPARC) Chemistry-Climate Model Initiative (CCMI) (Morgenstern et al., 2017). For each type of simulation we consider an ensemble of three members in order to better extract the forced signal by averaging the ensemble members. The first ensemble is the REF-C2 of CCMI, which follows the WMO A1 scenario for ozone depleting substances (ODS), and the RCP6.0 for the other greenhouse gases (GHG), tropospheric ozone precursors, and aerosol emissions (Meinshausen et al., 2011). This is our control ensemble. The second ensemble is the sensitivity experiment SEN-C2-fODS2000 of CCMI, and it is identical to REF-C2, except for the fact that ODS are fixed at 2000 levels. Therefore, in the SEN-C2-fODS2000 simulations there is a large ozone hole that does not recover in the 21st century. The third ensemble follows the RCP8.5 scenario for GHG emissions instead of the RCP6.0 and the WMO A1 scenario for ODS. We note that all results discussed here are robust in all ensemble members.

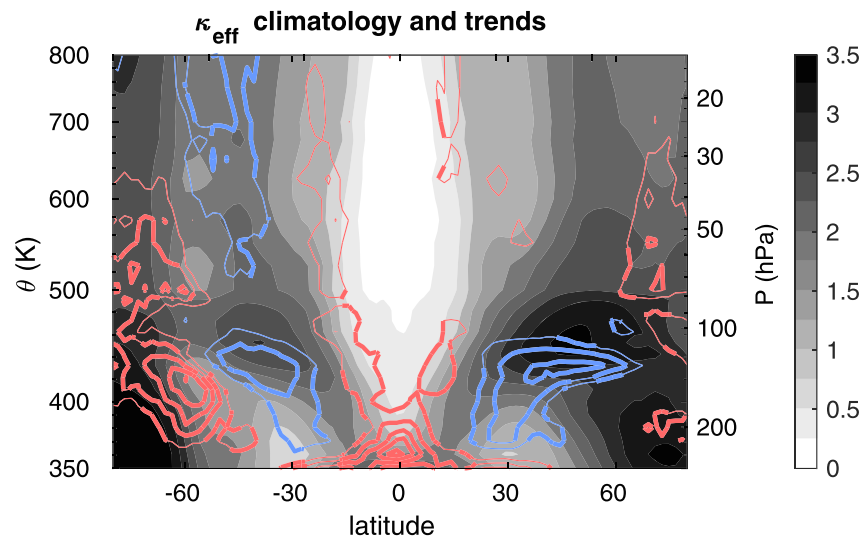


Figure 1. Climatology (shading) and trends (contours; contour interval: 0.01 decade^{-1} ; red/blue: positive/negative) of κ_{eff} for the ensemble mean of RCP6.0 simulations for the annual mean 2002–2009. Thick contours denote statistically significant trends with 95% confidence level using a Student's t test. Approximate pressure levels are included for reference.

The effective diffusivity (Haynes & Shuckburgh, 2000; Nakamura, 1996), κ_{eff} , is a diffusion coefficient defined in equivalent latitude coordinates that reflects the elongation of tracer contours associated with irreversible diffusion across the contour. In this study, we will work with the normalized equivalent length squared, which is a nondimensional quantity proportional to the effective diffusivity, $\Lambda_{\text{eq}} = \kappa_{\text{eff}}/\kappa$, where the diffusion coefficient κ depends on the resolution of the model and the hyperdiffusion scheme employed. For simplicity, because we are interested only in trends and not in the exact magnitude, we will refer to our results as effective diffusivity, or κ_{eff} . However, note that in all figures, the plotted magnitude is the natural logarithm of Λ_{eq} , which is a dimensionless quantity. While κ_{eff} is ideally computed from a passive tracer advected by the nondivergent flow on isentropes (Nakamura, 1996), in the present study we use the distribution of potential vorticity (PV), assuming that it behaves reasonably similar to a passive tracer in the stratosphere (see Abalos, Legras, & Shuckburgh, 2016, and Abalos, Randel, & Birner, 2016, for a discussion on this assumption).

3. Results

Figure 1 shows the annual mean trends in κ_{eff} for the ensemble mean of the reference simulation over the 21st century (contours), as well as the climatology for the first 30 years (shading). The climatology highlights regions of weak κ_{eff} corresponding to the tropical pipe in the stratosphere and the core of the subtropical jets. The location of the polar night jets (around 60°S and poleward of 60°N) can also be distinguished as bands of reduced κ_{eff} . Negative trends are observed on the equatorward and upper flank of the subtropical jets. The location of the negative trends in a region of climatologically strong mixing above the subtropical jets implies an upward extension of the transport barriers. On the other hand, positive trends are observed in the boundaries of the tropical pipe, most significantly in the lowermost stratosphere but extending to the entire altitude range in consideration (up to 800 K, or approximately 10 hPa). Finally, there are positive κ_{eff} trends in the SH lower stratosphere polar cap below 600 K and negative trends in SH middle latitudes above that level. In the next two subsections we analyze the trends above the subtropical jets and the SH polar region in more detail.

3.1. Trends Above the Subtropical Jets

There is a strong connection between the trends in κ_{eff} and the trends in the zonal wind. Figure 2a shows that the reduced κ_{eff} in the lower stratosphere subtropics and midlatitudes coincides with the strengthening of the upper flanks of the subtropical jets (black contours). These trends extend from fall to spring in each hemisphere and are collocated with a tightening of PV contours, shown by the PV gradient trends

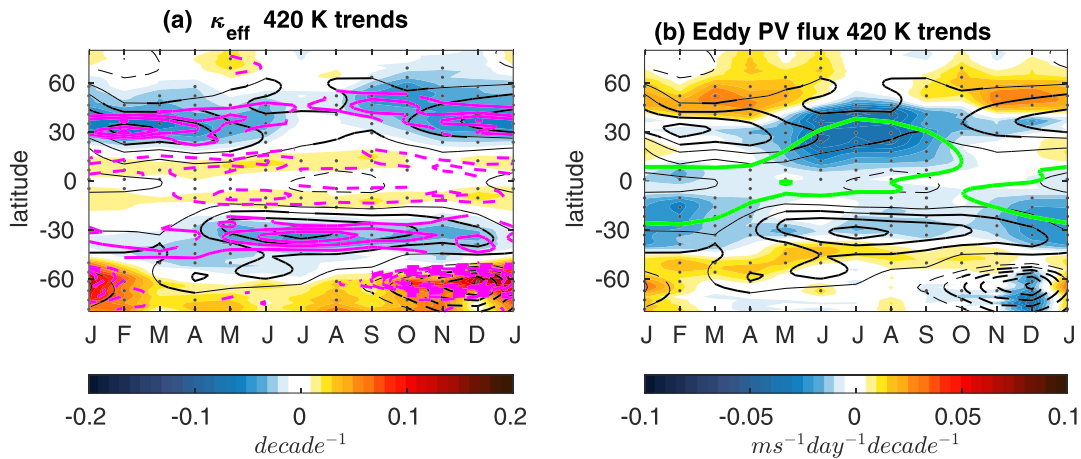


Figure 2. Latitude-month evolution at 420 K of trends in (a) κ_{eff} (shading), zonal wind (black; ci: 0.1 m/s/decade, solid: positive, dashed: negative) and PV gradient (magenta; ci: 0.25×10^{-7} PVU/m/decade, solid: positive, dashed: negative); (b) meridional eddy PV flux (shading) and zonal wind (black). The climatological zonal wind zero line is shown in green. Dots indicate statistically significant trends in shaded variables.

in Figure 2a (magenta contours). Hence, the trends in κ_{eff} are closely coupled to the strengthening of the subtropical transport barriers in the upper part of the climatological jets.

As mentioned in section 1, in association with the subtropical jet trends there is an upward and equatorward shift of the critical lines for Rossby waves (Shepherd & McLandress, 2011). Figure 2b shows the trends in meridional eddy PV flux on isentropic coordinates, which are almost identical to the trends in the Eliassen-Palm flux divergence (see Andrews et al., 1987) and thus depict changes in wave drag. It is clear from Figure 2b that the seasonality of the trends in the eddy PV flux (or wave drag) is different, and largely out of phase, with respect to that in κ_{eff} . The wave drag is enhanced (i.e., negative trends) in the subtropics and middle latitudes in summer of each hemisphere, when the background wind is weak and near-stationary Rossby waves meet their critical lines (the position of the zero wind line is included for reference in Figure 2b). In the other seasons, positive (negative) eddy PV flux trends are seen on the poleward (equatorward) side of the westerly trends, implying an equatorward shift of wave drag. The seasonality seen at this level for κ_{eff} and the eddy PV flux is representative of the general behavior in the lower stratosphere, as shown in Figures S1 and S2 of the supporting information.

Figure 2 emphasizes that κ_{eff} trends respond to the enhanced PV gradients and associated transport barriers (stronger in winter) rather than to the trends in wave drag (stronger in summer). However, enhanced wave breaking leads to more frequent irreversible contour elongation and thus potentially to enhanced molecular mixing and increased κ_{eff} . To further explore the connection between wave drag and κ_{eff} trends, it is useful to refer to the eddy diffusivity K_{yy} , a diffusion coefficient of the flow based on the flux-gradient relationship (Garcia, 1991; Plumb & Mahlman, 1987):

$$K_{yy} = -\frac{\overline{\langle \sigma \hat{v} \hat{P} \rangle}}{\langle \partial \hat{P} / \partial y \rangle}.$$

In this definition, angle brackets indicate time averages, which in this case are carried out over 1 season $\hat{A} = \overline{\sigma \hat{A}} / \bar{\sigma}$, where σ is the density on isentropes and overbars indicate zonal average. This expression therefore connects K_{yy} to the meridional eddy PV flux, closely related to the wave drag. Importantly, the term connecting the two is the meridional PV gradient, which reflects the strength of the jet. While both K_{yy} and κ_{eff} are defined to capture the regions of the flow potential to mix air masses, their very different methods of calculation imply they do not necessarily coincide. This is especially true for highly transient situations such as sudden stratospheric warmings (see de la Cámara et al., 2018), given that κ_{eff} is a Lagrangian quantity and K_{yy} is a Eulerian-mean diagnostic. However, the long-term averaged K_{yy} has been shown to provide a reasonable approximation of the main features of κ_{eff} (Abalos, Randel, & Birner, 2016).

Figure 3 shows the DJF trends in κ_{eff} , K_{yy} , PV flux, and PV gradient, overlaid by the zonal wind climatology and trends. The results for JJA are generally equivalent, exchanging hemispheres (Figure S3). The trends in K_{yy} (Figure 3b) exhibit qualitative similarities to κ_{eff} (Figure 3a), in particular negative trends in the upper

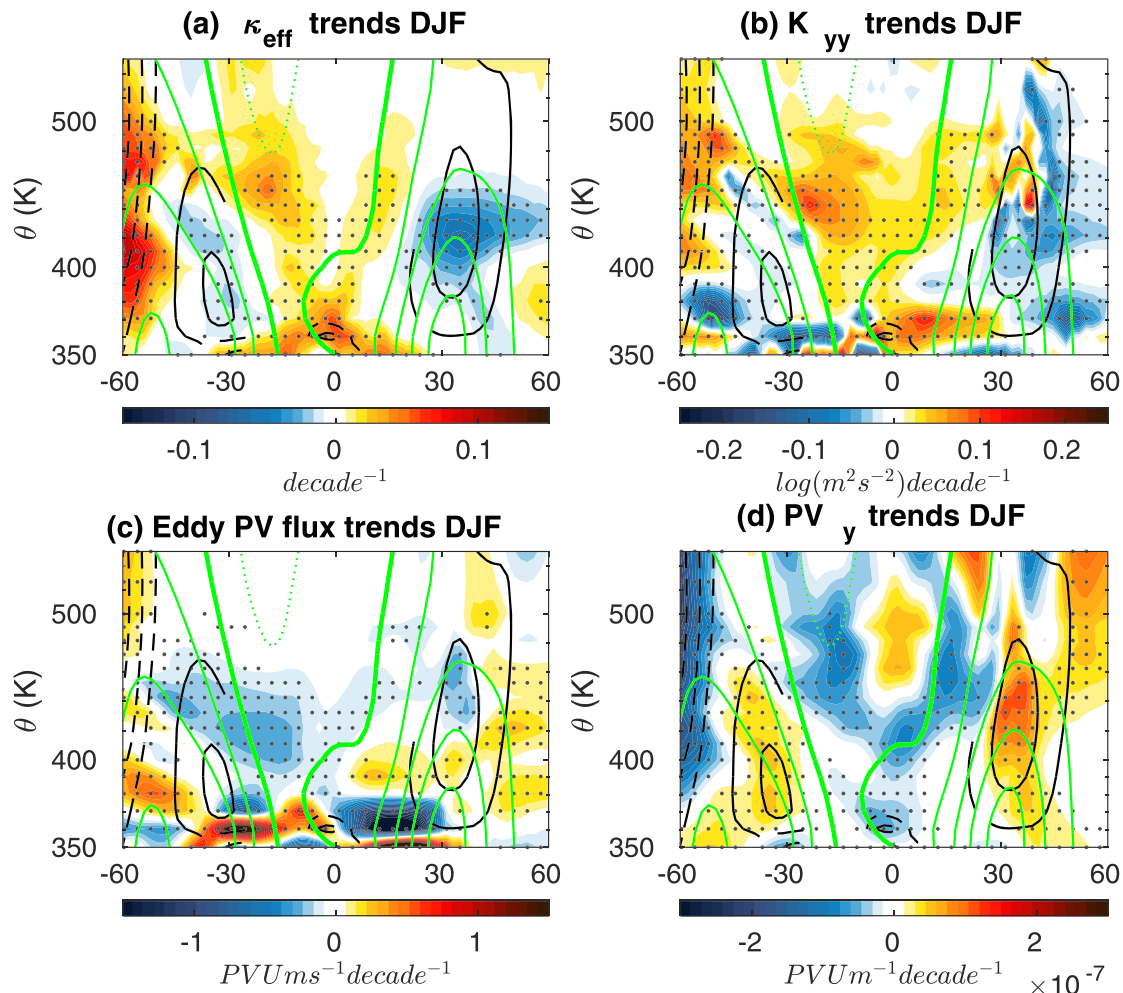


Figure 3. DJF trends in (a) κ_{eff} , (b) K_{yy} , (c) eddy PV flux, and (d) PV meridional gradient. Dots indicate statistically significant trends. Black contours: zonal wind trends (ci: 0.1 m/s/decade; only statistically significant trends shown; solid: positive, dashed: negative). Green: climatological zonal wind (ci: 10 m/s; thick contour: 0 m/s).

flanks of the subtropical jets extending into middle latitudes (strongest in winter) and positive trends in the tropics, around the zero wind lines. The eddy PV flux trends (Figure 3c) are negative, implying increased downgradient flux or wave drag, in the upper and equatorward flanks of the subtropical jets (strongest in summer), extending into the tropics around the zero wind lines. Positive trends are seen poleward and at lower levels with respect to the negative trends. These trends reflect the expected upward and equatorward shift in wave breaking, associated with the shift of critical lines (Shepherd & McLandress, 2011). What has not been highlighted before is that the enhanced wave drag maximizes in the summer lower stratosphere, when the climatological zero wind lines are lower. Moreover, the annual maximum wave drag increase is found in the boreal summer subtropics (Figures 2b, S2, and S3). On the other hand, the PV gradient trends (Figure 3d) are positive in the region of westerly trends and maximize in winter (cf. Figure 2a). In contrast, they are negative in the tropics around the zero wind lines, forming a dipole that reflects the upward and equatorward shift of the background PV structure.

The combined trends in both terms explain the sign of K_{yy} trends and by analogy help interpret the sign of κ_{eff} trends. We note that, while changes in κ_{eff} may in turn cause changes in the PV gradients in general, here the latter primarily respond to the external forcing (GHG increase), and thus we neglect this feedback to first order. In the winter subtropics ($\sim 30^\circ\text{N}$) the PV gradient increase dominates over the weak increase in (negative) PV flux, such that K_{yy} is reduced. Poleward of the jet, the (negative) PV flux decreases, and thus, both terms contribute to decrease K_{yy} . In the summer subtropics ($\sim 30^\circ\text{S}$), despite the strengthening of the eddy PV flux, the increase in PV gradients dominates resulting in weak negative K_{yy} trends. In contrast,

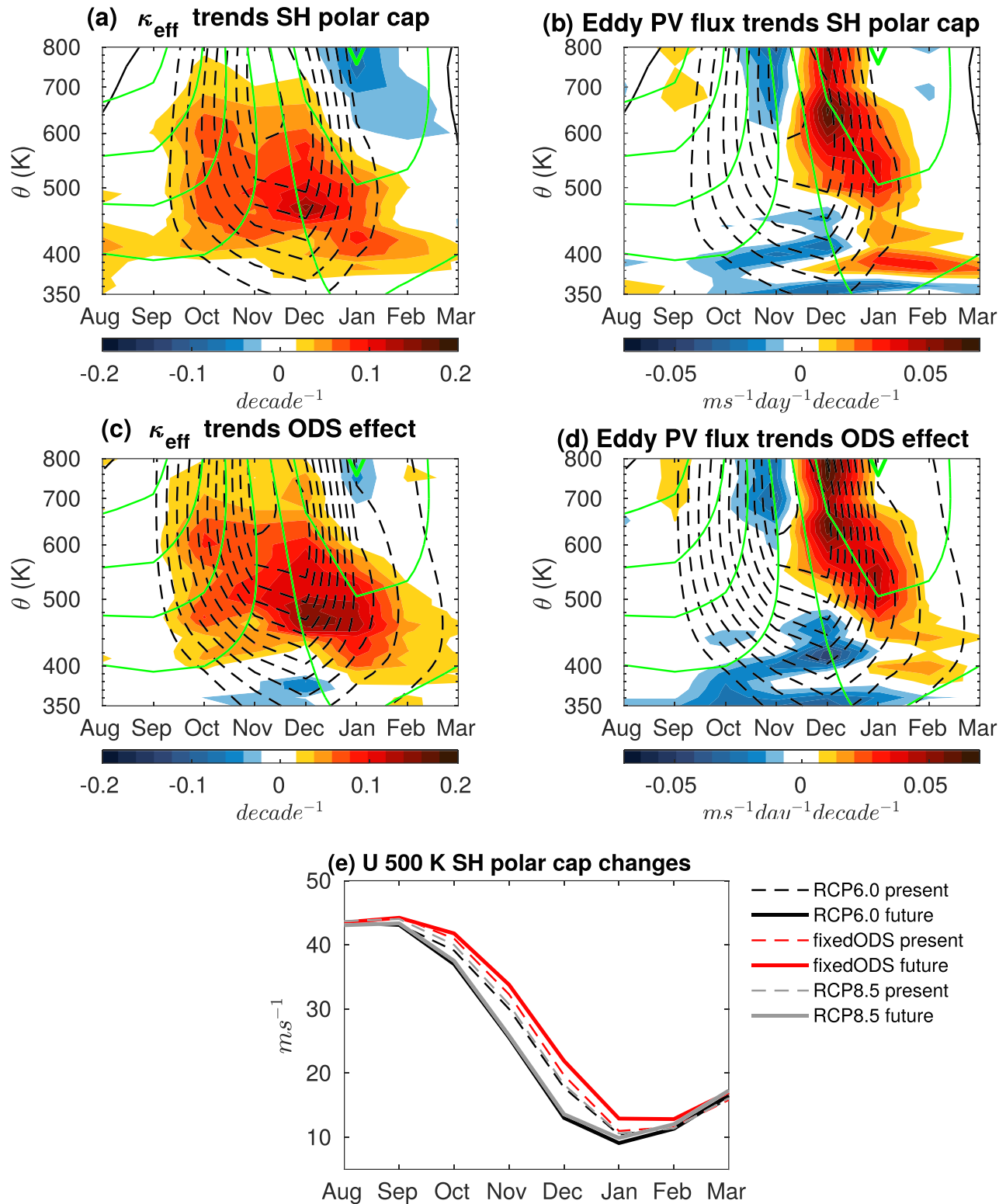


Figure 4. Trends in κ_{eff} (a and c) and eddy PV flux (b and d) averaged over (90–50°S) for RCP6.0 (a and b) and for the difference RCP6.0 minus SEN-C2-fODS2000 (c and d). Green: climatological zonal wind (ci: 10 m/s/decade). Black: zonal wind trends (ci: 0.1 m/s/decade). Solid: positive, dashed: negative. (e) SH polar vortex strength in the first (present) and last (future) 20 years of the 21st century.

in the tropics around the zero wind line in both hemispheres, the PV gradient decreases, and both terms contribute to increase K_{yy} (and thus κ_{eff}).

Therefore, the analogy between κ_{eff} and the eddy diffusivity K_{yy} confirms that κ_{eff} trends are controlled to a large extent by trends in PV gradient. Importantly, this implies that κ_{eff} trends above the subtropical jets provide information on the changes in transport barriers, but not on the eddy fluxes. In particular, the effect of strengthened transport barriers does not translate into reduced two-way mixing because it is compensated by the concomitant strengthening of PV gradients. Consistently, annual mean isentropic eddy transport in the lower stratosphere increases for tracers of tropospheric and stratospheric origin (Abalos et al., 2017, 2020). The trends in eddy tracer and PV fluxes show the same strong seasonality, not found in the κ_{eff} trends (cf. Figure 2).

To explore the dependency of the results of this section on the pathway of GHG emissions throughout the century, we examined the trends in a more extreme scenario, the RCP8.5. The trends above the subtropical jets of both hemispheres are qualitatively consistent and stronger than those in RCP6.0 (not shown). In particular, the wind, κ_{eff} and eddy PV flux trends are larger by approximately a factor of 2 in the more extreme climate change scenario (Figure S4).

3.2. Trends in the Antarctic Lower Stratosphere

Figure 1 highlights a region of positive annual mean κ_{eff} trends in the polar austral lower stratosphere and a region of negative trends in the austral middle stratosphere. Here we demonstrate that these trends are due to the ozone hole recovery. Figures 4a and 4b show the trends in κ_{eff} and eddy PV flux, respectively, averaged over the SH polar cap as a function of time and altitude. To examine the impact of ozone recovery on these trends, Figures 4c and 4d show the difference between the trends in the ensemble mean of the reference simulations minus that of the simulations with ODS fixed to 2000 levels. It is clear by comparing the top and middle panels that the net trends in this region are dominated by the effect of ODS. As ODS are phased out in the 21st century thanks to the Montreal Protocol, ozone concentrations rise and the polar stratosphere warms more rapidly in spring, which leads to a weaker and shorter-lived polar vortex. The tendency toward an earlier vortex spring breakdown is seen in the negative wind trends overlaid to the climatological seasonal weakening of the vortex in Figures 4a–4d.

Associated with this weakening trends of the vortex, there is enhanced κ_{eff} (Figures 4a and 4c). The κ_{eff} trends extend throughout the column in September–December and are confined to lower levels as the season progresses, peaking in the lower stratosphere from November to February. This downward progression follows the seasonal weakening of the background wind, with easterlies appearing above 600 K in December–January. The shift toward an earlier polar vortex breakup is evidenced in the wave drag at upper levels, which is strengthened in October–November and reduced in December–January (Figures 4b and 4d). In addition, there is enhanced wave drag in the lower stratosphere, which forms a dipole with the reduced drag at upper levels in December–January, consistent with inhibited upward Rossby wave propagation as critical lines descend. Coherently, κ_{eff} features positive trends below 600 K and negative trends above that level near the zero wind contour (Figures 4b and 4d). The negative κ_{eff} trends are the strongest in middle latitudes above 600 K (Figure S1a). Therefore, wave drag and κ_{eff} trends in the Antarctic polar stratosphere both respond to the descent of the critical lines for Rossby wave breaking associated with the ozone hole recovery in austral summer. This behavior is consistent with that shown in Abalos et al. (2019), where mirror but opposite sign κ_{eff} trends were found for the ozone hole formation period. Recent work has shown that increasing GHG strengthen the SH polar vortex and delay its breakdown (Ceppi & Shepherd, 2019). To contrast the impacts of GHG and ODS, Figure 4e shows the 21st century change in zonal wind speed in the lower stratosphere SH polar cap for the ensemble means of RCP6.0, fixed-ODS-2000, and RCP8.5 scenarios. By the end of the century, the vortex wind speeds are notably higher in the simulation without ozone recovery than in the other two. Hence, the weakening effect of ODS outweighs the strengthening effect of GHG on the SH polar vortex. Moreover, this is also true in the more extreme climate change scenario RCP8.5, where the vortex strength is reduced almost as much as in RCP6.0.

4. Conclusions

We have shown that the subtropical transport barriers extend to higher levels in the 21st century in response to the strengthening of the upper flanks of the subtropical jets. Nevertheless, isentropic eddy transport is

enhanced at the edges of the tropical pipe in the lower stratosphere, due to the upward and equatorward shift in wave drag following the critical lines, consistent with the mechanism proposed by Shepherd and McLandress (2011). While enhanced Rossby wave breaking is potentially associated with larger tracer contour elongation, we find little correspondence between κ_{eff} and eddy PV flux trends, especially in terms of seasonality. Eddy transport is enhanced mostly in the summer lower stratosphere, where the critical line effect is dominant due to the vicinity of the zero wind line. κ_{eff} trends are tightly coupled to those in zonal wind and PV gradients in the upper flanks of the winter mixing barriers, which extend from fall to spring. In the tropical lower stratosphere, near the climatological zero wind lines, both κ_{eff} and wave drag are enhanced in the annual mean. The recent CCMi multimodel study by Eichinger et al. (2019) examines K_{yy} annual mean trends and concludes that they reflect the upward and equatorward shift in wave drag. Here, we show that the dipolar patterns in the trends of κ_{eff} and eddy PV flux actually feature different seasonality. This discrepancy highlights the important role of tracer gradients in addition to transport barriers for understanding two-way mixing trends.

In addition to the response to climate change in the subtropical lower stratosphere, a strong signal is identified in the SH polar stratosphere, linked to the ozone hole recovery in the 21st century. κ_{eff} in the SH polar cap is enhanced from September to February as the polar vortex recovers its shorter and weaker character as compared to the beginning of the century. The effect of the ozone hole recovery extends to the SH polar and middle latitudes, where changes in wave drag associated with the descent of the critical line lead to weaker κ_{eff} above 600 K, and vice versa. This effect of ozone recovery overcomes the opposing effect of GHG on the vortex strength and breakdown date recently discussed by Ceppi and Shepherd (2019), even in the strong GHG emissions scenario RCP8.5.

The present work sheds light on the largely unexplored isentropic mixing trends, and the results highlight the usefulness of combining complementary transport diagnostics. The use of Lagrangian and Eulerian diagnostics emphasizes the complex interplay between wave drag, transport barriers, and tracer gradients. Evaluation of these processes against observations can help improve the representation of tracer variability and trends in chemistry-climate models.

Data Availability Statement

The simulations used in this study are publicly available (at <https://www2.acom.ucar.edu/gcm/ccmi-output>).

Acknowledgments

We acknowledge insightful comments from Hella Garny and an anonymous reviewer that have helped improve the paper. This study has been funded by the Spanish Ministry of Science and Innovation under grants CGL2017-83198-R (STEADY) and PID2019-109107GB-I00 (DYNWARM) and by the Santander-UCM grant PR87/19-22679 (STRATWARS). MA is supported by the Program Atracción de Talento de la Comunidad de Madrid (2016-T2/AMB-1405). We are thankful to D. Kinnison (NCAR) for carrying out the WACCM simulations. The authors acknowledge support from NCAR and CISL high-performance computing (HPC) systems.

References

- Abalos, M., Legras, B., & Shuckburgh, E. (2016). Interannual variability in effective diffusivity in the upper troposphere/lower stratosphere from reanalysis data. *Quarterly Journal of the Royal Meteorological Society*, 142(697), 1847–1861.
- Abalos, M., Orbe, C., Kinnison, D. E., Plummer, D., Oman, L. D., Jöckel, P., et al. (2020). Future trends in stratosphere-to-troposphere transport in CCMi models. *Atmospheric Chemistry and Physics*, 20(11), 6883–6901.
- Abalos, M., Polvani, L., Calvo, N., Kinnison, D., Ploeger, F., Randel, W., & Solomon, S. (2019). New insights on the impact of ozone-depleting substances on the Brewer-Dobson circulation. *Journal of Geophysical Research: Atmospheres*, 124, 2435–2451. <https://doi.org/10.1029/2018JD029301>
- Abalos, M., Randel, W. J., & Birner, T. (2016). Phase-speed spectra of eddy tracer fluxes linked to isentropic stirring and mixing in the upper troposphere and lower stratosphere. *Journal of the Atmospheric Sciences*, 73(12), 4711–4730.
- Abalos, M., Randel, W. J., Kinnison, D. E., & Garcia, R. R. (2017). Using the artificial tracer e90 to examine present and future UTLS tracer transport in WACCM. *Journal of the Atmospheric Sciences*, 74, 3383–3403.
- Andrews, D. G., Holton, J. R., & Leovy, C. B. (1987). *Middle atmosphere dynamics*. San Diego, California: Academic Press.
- Ball, W. T., Alsing, J., Mortlock, D. J., Staehelin, J., Haigh, J. D., Peter, T., et al. (2018). Evidence for a continuous decline in lower stratospheric ozone offsetting ozone layer recovery. *Atmospheric Chemistry and Physics*, 18(2), 1379–1394.
- Butchart, N. (2014). The Brewer-Dobson circulation. *Reviews of Geophysics*, 52, 157–184. <https://doi.org/10.1002/2013RG000448>
- Ceppi, P., & Shepherd, T. G. (2019). The role of the stratospheric polar vortex for the austral jet response to greenhouse gas forcing. *Geophysical Research Letters*, 46, 6972–6979. <https://doi.org/10.1029/2019GL082883>
- Chipperfield, M. P., Dhomse, S., Hossaini, R., Feng, W., Santee, M. L., Weber, M., et al. (2018). On the cause of recent variations in lower stratospheric ozone. *Geophysical Research Letters*, 45, 5718–5726. <https://doi.org/10.1029/2018GL078071>
- de la Cámara, A., Abalos, M., & Hitchcock, P. (2018). Changes in stratospheric transport and mixing during sudden stratospheric warmings in reanalysis and model. *Journal of Geophysical Research: Atmospheres*, 123, 3356–3373. <https://doi.org/10.1002/2017JD028007>
- Eichinger, R., Dietmüller, S., Garny, H., Šácha, P., Birner, T., Bönisch, H., et al. (2019). The influence of mixing on the stratospheric age of air changes in the 21st century. *Atmospheric Chemistry and Physics*, 19(2), 921–940.
- García, R. R. (1991). Parameterization of planetary wave breaking in the middle atmosphere. *Journal of the Atmospheric Sciences*, 48, 1405–1419.
- García, R. R., & Randel, W. J. (2008). Acceleration of the Brewer-Dobson circulation due to increases in greenhouse gases. *Journal of the Atmospheric Sciences*, 65(8), 2731–2739.
- García, R. R., Smith, A. K., Kinnison, D. E., de la Cámara, A., & Murphy, D. J. (2017). Modification of the gravity wave parameterization in the whole atmosphere community climate model: Motivation and results. *Journal of the Atmospheric Sciences*, 74(1), 275–291.

- Haynes, P., & Shuckburgh, E. (2000). Effective diffusivity as a diagnostic of atmospheric transport: 1. Stratosphere. *Journal of Geophysical Research*, 105(D18), 22,777–22,794.
- Li, F., Waugh, D. W., Douglass, A. R., Newman, P. A., Strahan, S. E., Ma, J., et al. (2012). Long-term changes in stratospheric age spectra in the 21st century in the Goddard Earth Observing System Chemistry-Climate Model (GEOSCCM). *Journal of Geophysical Research*, 117, D20119. <https://doi.org/10.1029/2012JD017905>
- Marsh, D. R., Mills, M. J., Kinnison, D. E., Lamarque, J. F., Calvo, N., & Polvani, L. M. (2013). Climate change from 1850 to 2005 simulated in CESM1 (WACCM). *Journal of Climate*, 26(19), 7372–7391.
- McLandress, C., Jonsson, A. I., Plummer, D. A., Reader, M. C., Scinocca, J. F., & Shepherd, T. G. (2010). Separating the dynamical effects of climate change and ozone depletion. Part I: Southern hemisphere stratosphere. *Journal of Climate*, 23(18), 5002–5020.
- Meinshausen, M., Smith, S. J., & Calvin, K. (2011). The RCP greenhouse gas concentrations and their extensions from 1765 to 2300. *Climatic Change*, 109, 213.
- Morgenstern, O., Hegglin, M. I., Rozanov, E., O'Connor, F. M., Abraham, N. L., Akiyoshi, H., et al. (2017). Review of the global models used within phase 1 of the Chemistry-Climate Model Initiative (CCMI). *Geoscientific Model Development*, 10(2), 639–671.
- Nakamura, N. (1996). Two-dimensional mixing, edge formation, and permeability diagnosed in an area coordinate. *Journal of the Atmospheric Sciences*, 53(11), 1524–1537.
- Oman, L., Waugh, D. W., Pawson, S., Stolarski, R. S., & Newman, P. A. (2009). On the influence of anthropogenic forcings on changes in the stratospheric mean age. *Journal of Geophysical Research*, 114, D03105. <https://doi.org/10.1029/2008JD010378>
- Orbe, C., Wargan, K., Pawson, S., & Oman, L. D. (2020). Mechanisms linked to recent ozone decreases in the Northern Hemisphere lower stratosphere. *Journal of Geophysical Research: Atmospheres*, 125, e2019JD031631. <https://doi.org/10.1029/2019JD031631>
- Ploeger, F., Abalos, M., Birner, T., Konopka, P., Legras, B., Müller, R., & Riese, M. (2015). Quantifying the effects of mixing and residual circulation on trends of stratospheric mean age of air. *Geophysical Research Letters*, 42, 2047–2054. <https://doi.org/10.1002/2014GL062927>
- Plumb, R. A. (2002). Stratospheric transport. *Journal of the Meteorological Society of Japan*, 80(4B), 793–809.
- Plumb, R. A., & Mahlman, J. D. (1987). The zonally averaged transport characteristics of the GFDL general circulation/transport model. *Journal of the Atmospheric Sciences*, 44(2), 298–327.
- Polvani, L. M., Abalos, M., Garcia, R., Kinnison, D., & Randel, W. J. (2018). Significant weakening of Brewer-Dobson circulation trends over the 21st century as a consequence of the montreal protocol. *Geophysical Research Letters*, 45, 401–409. <https://doi.org/10.1002/2017GL075345>
- Polvani, L. M., Wang, L., Abalos, M., Butchart, N., Chipperfield, M. P., Dameris, M., et al. (2019). Large impacts, past and future, of ozone-depleting substances on Brewer-Dobson circulation trends: A multimodel assessment. *Journal of Geophysical Research: Atmospheres*, 124, 6669–6680. <https://doi.org/10.1029/2018JD029516>
- Shepherd, T. G., & McLandress, C. (2011). A robust mechanism for strengthening of the Brewer-Dobson circulation in response to climate change: Critical-layer control of subtropical wave breaking. *Journal of the Atmospheric Sciences*, 68(4), 784–797.
- Solomon, S., Kinnison, D., Bandoro, J., & Garcia, R. (2015). Simulation of polar ozone depletion: An update. *Journal of Geophysical Research: Atmospheres*, 120, 7958–7974. <https://doi.org/10.1002/2015JD023365>
- Wargan, K., Orbe, C., Pawson, S., Ziemke, J. R., Oman, L. D., Olsen, M. A., et al. (2018). Recent decline in extratropical lower stratospheric ozone attributed to circulation changes. *Geophysical Research Letters*, 45, 5166–5176. <https://doi.org/10.1029/2018GL077406>
- World Meteorological Organization (WMO) (2018). Scientific assessment of ozone depletion: 2018. Geneva, Switzerland: Global Ozone Research and Monitoring Project Report No. 58. 588 pp.